J. Fluid Mech. (2009), *vol.* 621, *pp.* 59–67.
doi:10.1017/S0022112008004977 Printed in the United Kingdom

Lateral force on a rigid sphere in large-inertia laminar pipe flow

JEAN-PHILIPPE MATAS[1]†, JEFFREY F. MORRIS[2] AND ÉLISABETH GUAZZELLI[3]

[1]LEGI CNRS UMR 5519 – Université J. Fourier, BP 53 38041 Grenoble cedex 9, France
[2]Levich Institute and Chemical Engineering, City College of CUNY, New York, NY 10031, USA
[3]IUSTI CNRS UMR 6595 – Polytech' Marseille – Aix-Marseille Université (U1), 5 rue Enrico Fermi, 13453 Marseille cedex 13, France

(Received 2 July 2008 and in revised form 13 November 2008)

We present a prediction of the lateral force exerted on a rigid neutrally buoyant sphere in circular cross-section Poiseuille flow. The force is calculated with the method of matched asymptotic expansions. We investigate the influence of the pipe Reynolds number in the range 1–2000 on the equilibrium position and the magnitude of the lateral force. We show that the predicted lift force in a circular geometry is qualitatively similar to, but quantitatively different from, that in a plane channel. The predicted force in the pipe is significantly smaller than the channel result, and the zero of the force which determines the equilibrium radial position of a suspended particle lies closer to the centreline in the pipe.

1. Introduction

In 1962, Segré & Silberberg offered evidence of inertial migration of a rigid sphere in pipe flow: they observed that rigid neutrally buoyant spheres in Poiseuille flow migrated to an equilibrium position located at a radius of $r \approx 0.6R$, with R the radius of the pipe. The equilibrium position $0.6R$ was observed for Reynolds numbers $Re = 2R\bar{U}/\nu = O(1)$ and shifted to larger radius for larger Re. The Reynolds number is defined using $\bar{U}$ as the average axial velocity and ν as the kinematic viscosity. Recent experiments by Matas, Morris & Guazzelli (2004) confirmed that the equilibrium position moves towards the wall of the pipe as Re increases. However, a new observation was made: an additional equilibrium position was found at a radius $r_{inner} \approx 0.5R$. The majority of the particles were found to lie on this inner annulus for $Re > 700$.

The phenomenon of inertial particle migration impacts a range of applications, including microfluidic flows. This is perhaps surprising, as the effect of inertia on particle-laden flows has typically been studied in relatively large (centimetre scale) pipes, and the typical cross-section dimensions below 100 μm could lead one to the expectation that inertia is negligible. However, for low viscosity fluids such as water, $Re \geqslant 1$ is easily obtained even in small channels. For particles which occupy a significant fraction of the conduit cross-section, the resulting migration has been exploited in microfluidic devices to focus and sort particles or cells (Di Carlo *et al.* 2007). The present work addresses particles of vanishing size for analytical

† Email address for correspondence: matas@hmg.inpg.fr

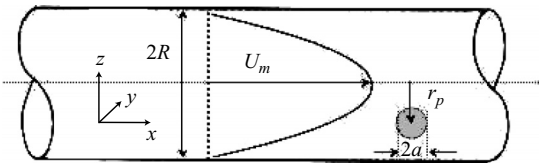

FIGURE 1. Basic parameters used in the description of pipe flow.

convenience, but the results will be shown to lead to the conclusion that finite size is a key consideration.

The pioneering work of Segré & Silberberg (1962) prompted several theoretical studies, based on concepts developed by Saffman (1965), which support the existence of an equilibrium position (Ho & Leal 1974; Schonberg & Hinch 1989; Hogg 1994). More recently, Asmolov (1999) extended the matched asymptotic approach of Schonberg & Hinch (1989) to higher Reynolds numbers (up to $Re = 1500$). He showed that the equilibrium position of Segré & Silberberg (1962) was shifted progressively towards the wall as Re increased but did not find a second equilibrium position. The question raised by Matas *et al.* (2004) was whether this discrepancy between theory and experiment with respect to the existence of the inner annulus is due to the finite particle size (and hence the finiteness of the particle Reynolds number) in the experiment or to the pipe geometry. All theories to date were investigated for a point particle in plane Poiseuille flow. The small parameter in the asymptotic expansion is $\epsilon = \sqrt{R_p}$, where the particle Reynolds number is defined as $R_p = (Re/2)(a/R)^2$ with a the radius of the particle.

With the goal of clarifying the cause of the discrepancy between theory and experimental observation in the problem of inertial migration, we examine the predicted lateral force for a circular cross-section pipe. To do so, we have extended the matched asymptotic expansion calculation, developed and previously applied for a plane channel, to the cylindrical geometry. We begin by presenting the analysis leading to a fourth-order differential equation for the sphere lateral velocity. Then we discuss the lateral force obtained after these equations are integrated and compare the particle equilibrium position predicted as a zero of this lateral force to the experimental observations.

2. Method

The lateral force is obtained via the method of matched asymptotic expansion, developed for the channel geometry by Schonberg & Hinch (1989), Hogg (1994) and Asmolov (1999) and used to evaluate the lift force on a spherical rigid particle in a plane Poiseuille flow. Here, the method is extended to pressure-driven flow in a cylindrical geometry. The details of the method are presented in the references noted, but we outline the ideas specific to the case considered here. The parabolic flow is disturbed by a neutrally buoyant rigid sphere of radius a located at a distance r_p from the pipe axis (see figure 1). The method assumes the particle-scale inertia is small, $R_p \ll 1$, and thus the flow near the suspended sphere (in the 'inner region') is given at leading order by a Stokes flow solution. Far from the particle, in the 'outer region' at a distance of $O(aR_p^{-1/2})$, a balance of advection and diffusion requires consideration of the Oseen equations. The boundary conditions associated with the specific geometry considered must be accounted for by enforcing noslip at the pipe boundary in the present calculation. The inner solution is needed only at leading

order for the matching with the outer solution, and the particle is thus represented by its leading-order force moment, which for the force- and torque-free sphere considered here is the flow due to a stresslet (symmetric force dipole). We do not consider here the case of a dense particle for which the leading-order solution is the point force solution or Stokeslet. This case has been treated for the channel geometry (Hogg 1994; Asmolov 1999).

We begin by considering a Cartesian coordinate system fixed on the particle and develop the matched asymptotic problem in this frame. We then convert to the more natural cylindrical coordinates with origin at the centreline to solve the problem. The origin of the coordinate system is first taken at the centre of the sphere, thus moving with it, and the axes are oriented as shown in figure 1. We denote as $\boldsymbol{U}_p$ the slip velocity of the particle relative to the fluid, U_m the maximum velocity at the pipe centre and $\boldsymbol{v}_f$ the value of the unperturbed fluid velocity in a frame moving with the unperturbed fluid at the centre of the particle.

We introduce $\boldsymbol{u}$ as the perturbation velocity field induced by the particle on the fluid velocity. This perturbation velocity is the solution of the system

$$\frac{R_p}{\alpha}(\boldsymbol{u}\cdot\nabla\boldsymbol{u}+\boldsymbol{v}_f\nabla u+\boldsymbol{u}\cdot\nabla\boldsymbol{v}_f-\boldsymbol{U}_p\cdot\nabla\boldsymbol{u})=-\nabla p+\nabla^2\boldsymbol{u}, \tag{2.1}$$

$$\nabla\cdot\boldsymbol{u}=0, \tag{2.2}$$

$$\boldsymbol{u}=\boldsymbol{U}_p+(a/2R)\boldsymbol{\Omega}_p\times\boldsymbol{r}-\boldsymbol{v}_f \quad \text{at } \boldsymbol{r}=1, \tag{2.3}$$

$$\boldsymbol{u}=0 \quad \text{on the pipe wall}, \tag{2.4}$$

$$\boldsymbol{u}\to 0 \quad \text{for } |x|\to\infty, \tag{2.5}$$

where the position $\boldsymbol{r}$ is made dimensionless by a, velocities by U_m and the angular velocity $\boldsymbol{\Omega}_p$ by $U_m/2R$. We denote $\alpha = a/2R$ as the ratio of particle size to pipe diameter. Both $R_p = (2Re)\alpha^2$ and α are assumed to be small. In contrast, the pipe Reynolds number Re is of the order of unity or larger.

In the matched asymptotic expansion theory, two regions of the flow are considered. In the inner region close to the particle, the length scale is the particle radius a: in the limit of small R_p, the leading-order governing equations reduce to the Stokes equations. We consider a neutrally buoyant particle, for which the leading-order inner solution is the stresslet velocity field corresponding to viscous flow driven by a symmetric force dipole (see Schonberg & Hinch 1989; Asmolov 1999). In the outer region far from the particle, we must consider Oseen equations in which advection terms balance viscous terms. In this region, the new length scale is related to the inner length scale by a factor ϵ: $(X, Y, Z) = \epsilon(x, y, z)$. The stretching factor must be chosen so that inertial terms balance viscous terms in the equation for the velocity perturbation $\boldsymbol{u}$; so $\epsilon = R_p^{1/2}$ (Hogg 1994; Asmolov 1999).

In the outer region, we choose to express the fluid velocity in the frame (X, Y, Z) moving with the fluid velocity at the particle centre with

$$V_X = (\epsilon/\alpha)\boldsymbol{v}_f\cdot\hat{\boldsymbol{x}} = \gamma Z - 2\sqrt{2}Re^{-1/2}(Y^2+Z^2),$$

where $\gamma = 4r_p/R$ is the dimensionless shear rate at the particle centre. The equation for the velocity perturbation $\boldsymbol{u}$ now becomes

$$\left[V_X\frac{\partial\boldsymbol{u}}{\partial X}+\left(u_y\frac{\mathrm{d}V_X}{\mathrm{d}Y}+u_z\frac{\mathrm{d}V_X}{\mathrm{d}Z}\right)\hat{\boldsymbol{x}}\right]$$
$$=-\epsilon^{-1}\nabla p+\nabla^2\boldsymbol{u}-\frac{10}{3}\pi\gamma\alpha\epsilon^2\left[\frac{\partial\delta(\boldsymbol{R})}{\partial X}\hat{\boldsymbol{z}}+\frac{\partial\delta(\boldsymbol{R})}{\partial Z}\hat{\boldsymbol{x}}\right]. \tag{2.6}$$

where $\delta(\boldsymbol{R})$ refers to the delta function at the location $\boldsymbol{R} = (X, Y, Z)$, which appears in a form resulting from the stresslet forcing (Hogg 1994; Asmolov 1999).

The forcing term sets the scaling of velocity and pressure: $u \sim \alpha\epsilon^2 \sim \epsilon^3$ and $p \sim \epsilon^4$. We therefore introduce $\boldsymbol{U} = \epsilon^{-3}\boldsymbol{u}$ and $P = \epsilon^{-4}p$. We will also use the the velocity components (U, V, W) of $\boldsymbol{U}$. We now change coordinates and move to a frame (X', Y', Z') with its origin on the pipe axis, such that $X' = X$, $Y' = Y$ and $Z' = Z - Z_p$, where $Z_p = (r_p/\sqrt{2}R)Re^{1/2}$ is the distance from the particle to the cylinder axis in the outer region units. Fluid velocity in this frame is simply

$$V_X = \left[\left(r_p^2/R^2\right)(2Re)^{1/2} - 2\sqrt{2}R'^2/Re^{1/2}\right], \tag{2.7}$$

where $R' = \sqrt{Y'^2 + Z'^2}$ is the distance to the pipe axis. In particular, velocity is zero at the particle position: $V_X[R' = (r_p/R)(\sqrt{2}/2)Re^{1/2}] = 0$. Taking the divergence of (2.6) gives an expression for the Laplacian of pressure:

$$\nabla^2 P = -2\left(\frac{\partial V}{\partial X'}\frac{\partial V_X}{\partial Y'} + \frac{\partial W}{\partial X'}\frac{\partial V_X}{\partial Z'}\right) - \frac{20}{3}\frac{\pi\gamma}{(2Re)^{1/2}}\frac{\partial^2}{\partial X'\partial Z'}\delta(\boldsymbol{R}' - Z_p\hat{\boldsymbol{z}}). \tag{2.8}$$

With this expression, pressure can be eliminated from (2.6), yielding an equation for velocity only:

$$\nabla^2\left(V_X\frac{\partial W}{\partial X'}\right) = 2\frac{\partial}{\partial Z'}\left(\frac{\partial V}{\partial X'}\frac{\partial V_X}{\partial Y'} + \frac{\partial W}{\partial X'}\frac{\partial V_X}{\partial Z'}\right) + \nabla^2(\nabla^2 W) - \frac{10}{3}\frac{\pi\gamma}{(2Re)^{1/2}}\frac{\partial}{\partial X'}\left[\nabla^2\delta(\boldsymbol{R}' - Z_p\hat{\boldsymbol{z}}) - 2\frac{\partial^2}{\partial Z'^2}\delta(\boldsymbol{R}' - Z_p\hat{\boldsymbol{z}})\right]. \tag{2.9}$$

We next take the Fourier transform of the previous equation along the X direction. Lateral velocity is then expressed as

$$\tilde{W} = \frac{1}{2\pi}\int_{-\infty}^{+\infty} W e^{-\mathrm{i}k_x X'}\,\mathrm{d}X', \tag{2.10}$$

and (2.9) can be written

$$\mathrm{i}k_x\left(\frac{\partial^2}{\partial Y'^2} + \frac{\partial^2}{\partial Z'^2} - k_x^2\right)V_X\tilde{W} = 2\mathrm{i}k_x\frac{\partial}{\partial Z'}\left(\tilde{V}\frac{\partial V_X}{\partial Y'} + \tilde{W}\frac{\partial V_X}{\partial Z'}\right) + \nabla^2(\nabla^2\tilde{W}) - \mathrm{i}k_x\frac{5}{3}\frac{\gamma}{(2Re)^{1/2}}\left[\nabla^2\tilde{\delta}(\boldsymbol{R}' - Z_p\hat{\boldsymbol{z}}) - 2\frac{\partial^2}{\partial Z'^2}\tilde{\delta}(\boldsymbol{R}' - Z_p\hat{\boldsymbol{z}})\right]. \tag{2.11}$$

We now change variables and replace variables (Y', Z') by polar coordinates (r, θ) as shown in figure 2:

$$\begin{cases} r^2 = Y'^2 + Z'^2, \\ \tan\theta = Y'/Z'. \end{cases}$$

The lateral velocity $\tilde{W}$ is then expanded in a Fourier series:

$$\tilde{W}(r, \theta, k_x) = \sum_m \tilde{\tilde{W}}(r, m, k_x)e^{\mathrm{i}m\theta}.$$

In the rest of the analysis the double tilde will be omitted to simplify notation. The aim of the calculation is to express the lateral velocity $W(r, \theta, X)$ at the particle location, i.e. for $\theta = 0$. Therefore we can drop all the terms proportional to $\sin\theta$ in the Fourier expansion of (2.11).

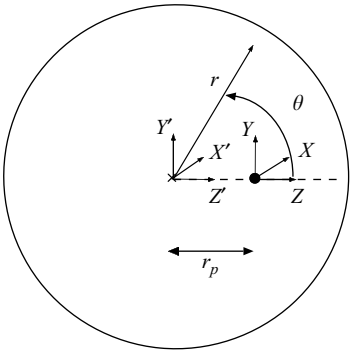

FIGURE 2. Coordinate systems used in the analysis.

The left-hand term of (2.11) can now be written

$$\mathrm{i}k_x\nabla^2(V_X W) = \mathrm{i}k_x\left[\partial_r^2 + \frac{1}{r}\partial_r - \left(k_x^2 + \frac{m^2}{r^2}\right)\right](V_X W).$$

The first term on the right-hand side of (2.11) becomes

$$2\mathrm{i}k_x\frac{\partial}{\partial Z'}\left(\tilde{V}\frac{\partial V_X}{\partial Y'} + \tilde{W}\frac{\partial V_X}{\partial Z'}\right) = 2\mathrm{i}k_x\partial_r(\tilde{W}\partial_r V_X).$$

The operator ∇^4 has to be expressed in cylindrical coordinates:

$$\nabla^4 = \partial_r^4 + \frac{2}{r}\partial_r^3 - \left[\frac{1}{r^2} + 2\left(k_x^2 + \frac{m^2}{r^2}\right)\right]\partial_r^2 + \left[\frac{1}{r^3} + \frac{4m}{r^3} - \frac{2}{r}\left(k_x^2 + \frac{m^2}{r^2}\right)\right]\partial_r + \left[-\frac{4m^2}{r^2} + \left(k_x^2 + \frac{m^2}{r^2}\right)^2\right]. \tag{2.12}$$

When the foregoing is inserted into (2.11), we obtain the following differential equation in r for the lateral velocity $W(r, m, k_x)$:

$$\begin{aligned}\partial_r^4 W + \frac{2}{r}\partial_r^3 W - \left[\frac{1}{r^2} + 2\left(k_x^2 + \frac{m^2}{r^2}\right) + \mathrm{i}k_x V_X(r)\right]\partial_r^2 W \\ + \left[\frac{1}{r^3} + \frac{4m}{r^3} - \frac{2}{r}\left(k_x^2 + \frac{m^2}{r^2}\right) - \mathrm{i}k_x\frac{V_X(r)}{r}\right]\partial_r W \\ + \left[-\frac{4m^2}{r^2} + \left(k_x^2 + \frac{m^2}{r^2}\right)^2 + \mathrm{i}k_x\left(\partial_r^2 V_X(r) - \frac{1}{r}\partial_r V_X(r) + \left(k_x^2 + \frac{m^2}{r^2}\right)V_X(r)\right)\right] W \\ = \mathrm{i}k_x\frac{5}{6}\frac{\gamma}{\pi(2Re)^{1/2}}\frac{1}{r_p}\left[\partial_r^2\delta + \frac{3}{r_p}\partial_r\delta + \left(\frac{3}{r_p^2} + k_x^2 + \frac{m^2}{r^2}\right)\delta\right],\end{aligned} \tag{2.13}$$

where the δ function is applied at the particle location. Boundary conditions at the nearest wall are

$$W(r = (2Re)^{1/2}/2, m, k_x) = 0,$$
$$\partial_r W(r = (2Re)^{1/2}/2, m, k_x) = 0.$$

The condition $\partial_r W = 0$ can be derived from mass conservation. A complementary set of conditions of the same form is taken on the other side of the particle: for $m \neq 0$

the conditions are applied at the centreline, while for $m = 0$ it is necessary to apply them at the opposite wall.

The forcing terms on the right-hand side of (2.13) are derived from the inner solution and its derivatives: following Saffman (1965), we consider them equivalent to discontinuities in the derivatives of the lateral velocity W. We denote respectively as Δ_1, Δ_2 and Δ_3 the jumps in the first, second and third derivatives of W. The lateral velocity and its jumps are then inserted into the left-hand side of (2.13), which yields

$$\nabla^4 W + 2\mathrm{i}k_x \partial_r (W \partial_r V_X) - \mathrm{i}k_x \nabla^2 (V_X W) = \text{regular terms}$$
$$+ \Delta_1 \partial_r^2 \delta + \left(\Delta_2 + \frac{2\Delta_1}{r_p} \right) \partial_r \delta + \left(\Delta_3 + 2\frac{\Delta_2}{r_p} + \frac{\Delta_1}{r_p^2} - 2\left(k_x^2 + \frac{m^2}{r_p^2} \right) \Delta_1 \right) \delta.$$

Identification with the right-hand side of (2.13) finally gives

$$\begin{cases} \Delta_1 = \mathrm{i}k_x \dfrac{5}{6} \dfrac{\gamma}{\pi (2Re)^{1/2}} \dfrac{1}{r_p}, \\ \Delta_2 = \dfrac{\Delta_1}{r_p}, \\ \Delta_3 = 3\left(k_x^2 + \dfrac{m^2}{r^2} \right) \Delta_1. \end{cases} \tag{2.14}$$

For fixed k_x and m, differential equation (2.13) is then integrated from the wall to the particle and from the centreline to the particle with a Runge–Kutta algorithm. The orthonormalization method used by Asmolov (1999) is employed to ensure a correct computation of the four independent solutions. (The method is detailed in the Appendix of Asmolov 1999.) The solutions found on each side are eventually connected across the particle via the discontinuities Δ_i given by (2.14), and the lateral velocity $W(r_p, m, k_x)$ is obtained. This velocity is integrated over m and k_x, to get the lateral velocity in real space $W(r_p, \theta = 0, X' = 0)$. The radially directed lift (or lateral) force is then just the Stokes drag $F = 6\pi\eta a W$ associated to this lateral velocity.

3. Results and conclusions

Figure 3(a) shows the lateral force F as a function of radial position for $1 \leqslant Re \leqslant 1750$. The magnitude of the lateral force is scaled by $\eta U_m a Re^{-1/2} \epsilon^3$. There is an important change in the shape of the curve as Re is increased: the curve flattens and develops a local minimum around $0.5R$, but no additional zero in the lateral force is found. We also note that the zero of the force is shifted towards the wall, in agreement with experimental observations and the channel flow predictions.

Figure 3(b–d) compares the predictions for pipe flow to those for channel flow (Asmolov 1999) for specific Reynolds numbers. Note that the particle location labelled r/R implies $2z/l$ for the channel geometry, where z is the distance from the centreline and l is the channel width. The magnitude of the lateral force is clearly smaller for the pipe calculation. For instance the maximum outward value for $Re = 30$ in figure 3(b), reached in both geometries around $r/R = 0.4$, is close to 2.9 in the planar case and 1.0 in the cylindrical case. The other significant difference is that the shift of the zero in lateral force towards the wall is smaller for the pipe calculation. This difference can be seen in figure 4, which shows the prediction for the equilibrium position in channel and pipe geometries in comparison with experimental data. The prediction from the present calculation appears to be in better agreement with experimental data. While

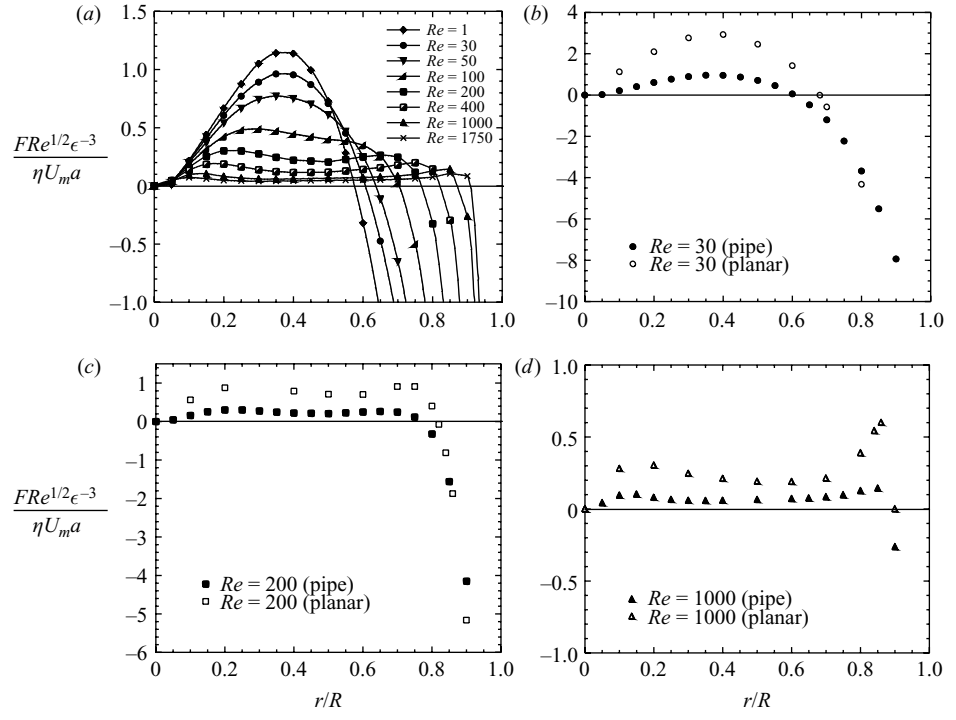

FIGURE 3. Lateral force: (*a*) pipe flow at various Re and comparison with channel cases for (*b*) $Re = 30$, (*c*) $= 200$ and (*d*) $= 1000$.

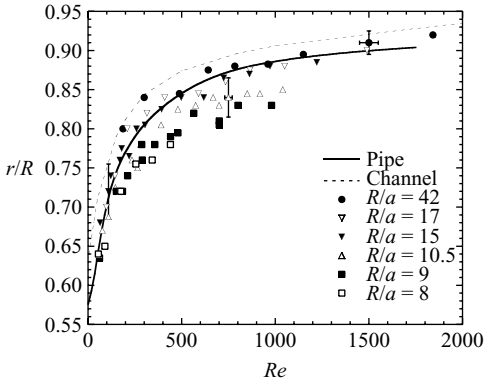

FIGURE 4. Comparison of the predicted equilibrium position for pipe (solid line) and channel (dotted line) theories with experimental data of Matas *et al.* (2004).

the curve from the channel calculation was uniformly above the experimental data, the curve from the pipe calculation passes among the data for smaller particles (large R/a).

There are two additional key findings in this work. The first is that the computed magnitude of the force decreases strongly with Re for either geometry and has importantly been found to be substantially smaller in the pipe geometry. This has consequences for the predicted entry length L_e of the inertial migration phenomenon. The asymptotic scaling for vanishing R_p (Matas *et al.* 2004) is given by $L_e/D \approx 6\pi A^{-1} Re^{-1} (R/a)^3$, where A is the typical magnitude (taken as the maximum of the

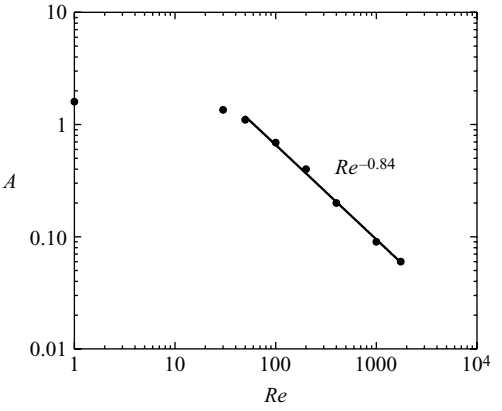

FIGURE 5. Variation of the scaled force amplitude A with Re. The line represents the best power law fit of the data for $50 \leqslant Re \leqslant 1750$.

outward force) of the scaled lateral force $FRe^{1/2}\epsilon^{-3}/(\eta U_m a)$. This scaling is poor as Re becomes large, because A decreases strongly as evidenced in figure 3(a). For the pipe, a power law fit of A yields $A \sim Re^{-0.84}$ for $50 \leqslant Re \leqslant 1750$ as shown in figure 5. This decrease nearly compensates the Re^{-1} dependence of the entry length scaling given above. Note, however, that for small Re, A tends to a constant value in agreement with the small Re theory, and hence $L_e \sim Re^{-1}$ as seen in Segré & Silberberg (1962). A further conclusion regarding the smaller amplitude in the pipe geometry is that it rationalizes the observation of Matas *et al.* (2004) that the large-Re channel-geometry theory seriously underestimates the observed entry length.

The second valuable finding is that there is, in fact, no new zero of the lateral force in the pipe geometry. This implies that the observation of an apparent bifurcation in the equilibrium position, with the appearance of an inner annulus in addition to the Segré–Silberberg equilibrium position, is most likely due to finite-size effects. An asymptotic analysis based on a point-particle representation, as performed here, is not able to capture this phenomenon. While the influence of finite-size effects on lift force in shear flows has been examined previously in numerical studies (Kurose & Komori 1999; Bagchi & Balachandar 2002), these are for cases in which the particle experiences finite force and torque. More closely related to the present study are recent numerical simulations (Shao, Yu & Sun 2008) of inertial migration of neutrally buoyant spherical particles in a periodic pipe flow, which find an inner annulus for elevated Re. These simulations use the fictitious domain method and were validated against small-Re migration problems (Yu & Shao 2007). Other numerical simulations using the lattice Boltzmann technique also find new equilibrium positions but are performed for a square conduit (Chun & Ladd 2006). The fact that we do not find a second zero of the lateral force, while the numerical simulation (Shao, Yu & Sun 2008) does indeed find a distribution of particles to an inner annulus, appears to confirm finite size as the basis for this phenomenon.

To summarize, we have applied a known technique based on matched asymptotic solutions to study inertial migration in the cylindrical geometry. By considering this geometry, we have filled a gap in the theoretical understanding of the problem. Relative to the results of the previous channel-flow theory, the new results for the cylindrical geometry are in better agreement with experimental observations (Matas *et al.* 2004) at elevated Reynolds numbers. In particular, the location of the zero

in force at finite radius in the pipe calculations lies closer to the centreline, and the magnitude of the lateral force is substantially smaller than the channel flow calculation predicts. The latter result rationalizes the observation of a longer entry length than predicted by the channel flow. The finding of only a single zero suggests that the second region of particle accumulation, at an inner annulus lying closer to the centreline, is a result of the finite size of the suspended particle.

REFERENCES

Asmolov, E. S. 1999 The inertial lift on a spherical particle in a plane Poiseuille flow at large channel Reynolds number. *J. Fluid Mech.* **381**, 63–87.

Bagchi, P. & Balachandar, S. 2002 Steady planar straining flow past a rigid sphere at moderate Reynolds number. *J. Fluid Mech.* **466**, 365–407.

Chun, B. & Ladd, A. J. C. 2006 Inertial migration of neutrally buoyant particles in a square duct: an investigation of multiple equilibrium positions. *Phys. Fluids* **18**, 031704.

Di Carlo, D., Irimia, D., Tompkins, R. G. & Toner, M. 2007 Continuous inertial focusing, ordering, and separation of particles in microchannels. *Proc. Natl. Acad. Sci. USA* **104**, 18892–18897.

Ho, B. P. & Leal, L. G. 1974 Inertial migration of rigid spheres in two-dimensional unidirectional flows. *J. Fluid Mech.* **65**, 365–400.

Hogg, A. J. 1994 The inertial migration of non-neutrally buoyant spherical particles in two-dimensional shear flows. *J. Fluid Mech.* **272**, 285–318.

Kurose, R. & Komori, S. 1999 Drag and lift forces on a rotating sphere in a linear shear flow. *J. Fluid Mech.* **384**, 183–206.

Matas, J.-P., Morris, J. F & Guazzelli, É. 2004 Inertial migration of rigid spherical particles in Poiseuille flow. *J. Fluid Mech.* **515**, 171–195.

Saffman, P. G. 1965 The lift on a small sphere in a slow shear flow. *J. Fluid Mech.* **22**, 385–400.

Schonberg, J. A. & Hinch, E. J. 1989 Inertial migration of a sphere in Poiseuille flow. *J. Fluid Mech.* **203**. 517–524.

Segré, G. & Silberberg, A. 1962 Behaviour of macroscopic rigid spheres in Poiseuille flow. Part 2. Experimental results and interpretation. *J. Fluid Mech.* **14**, 136–157.

Shao, X., Yu, Z. & Sun, B. 2008 Inertial migration of spherical particles in circular Poiseuille flow at moderately high Reynolds numbers. *Phys. Fluids* **20**, 103307.

Yu, Z. & Shao, X. 2007 A direct-forcing fictitious domain method for particulate flows. *J. Comp. Phys.* **227**, 292–314.